Biomimetic Superhydrophobic Surface of High Adhesion Fabricated with Micronano Binary Structure on Aluminum Alloy

ARTICLE *in* ACS APPLIED MATERIALS & INTERFACES · SEPTEMBER 2013

Impact Factor: 6.72 · DOI: 10.1021/am4014715 · Source: PubMed

6 AUTHORS, INCLUDING:

Yan Liu
Jilin University
7 PUBLICATIONS **56** CITATIONS
SEE PROFILE

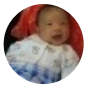

Jindan Liu
Jilin University
6 PUBLICATIONS **43** CITATIONS
SEE PROFILE

Shuyi Li
18 PUBLICATIONS **95** CITATIONS
SEE PROFILE

ACS APPLIED MATERIALS & INTERFACES

Research Article

www.acsami.org

Biomimetic Superhydrophobic Surface of High Adhesion Fabricated with Micronano Binary Structure on Aluminum Alloy

Yan Liu,*[,†] Jindan Liu,[†] Shuyi Li,[†] Jiaan Liu,[‡] Zhiwu Han,[†] and Luquan Ren[†]

[†]Key Laboratory of Bionic Engineering (Ministry of Education), Jilin University, Changchun 130022, P. R. China

[‡]Key Laboratory of Automobile Materials (Ministry of Education) and College of Materials Science and Engineering, Jilin University, Changchun 130022, P. R. China

ABSTRACT: Triggered by the microstructure characteristics of the surfaces of typical plant leaves such as the petals of red roses, a biomimetic superhydrophobic surface with high adhesion is successfully fabricated on aluminum alloy. The essential procedure is that samples were processed by a laser, then immersed and etched in nitric acid and copper nitrate, and finally modified by DTS ($CH_3(CH_2)_{11}Si(OCH_3)_3$). The obtained surfaces exhibit a binary structure consisting of microscale crater-like pits and nanoscale reticula. The superhydrophobicity can be simultaneously affected by the micronano binary structure and chemical composition of the surface.

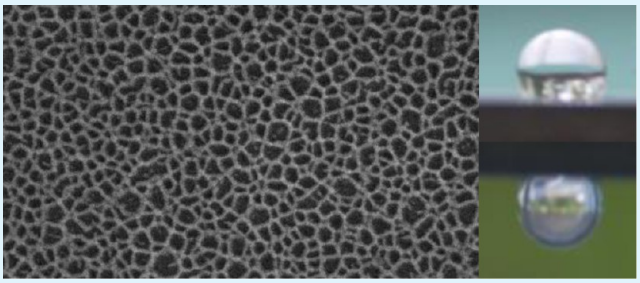

The contact angle of the superhydrophobic surface reaches up to 158.8 ± 2°. Especially, the surface with micronano binary structure is revealed to be an excellent adhesive property with petal-effect. Moreover, the superhydrophobic surfaces show excellent stability in aqueous solution with a large pH range and after being exposed long-term in air. In this way, the multifunctional biomimetic structural surface of the aluminum alloy is fabricated. Furthermore, the preparation technology in this article provides a new route for other metal materials.

KEYWORDS: *biomimetic, superhydrophobicity, adhesion, aluminum alloy, laser processing, chemical etching*

1. INTRODUCTION

Through evolution, nature has experimented with various solutions to overcome its challenges, which provide ready answers to scientific and technical problems.[1] Fortunately, many plant leaves exhibit excellent superhydrophobic properties, such as lotus leaves, rose petals, marigolds, and so forth. The micronano binary structure and chemical composition of surfaces endow them with water-repellent and self-cleaning or high adhesive force.[2−8] Therefore, the "lotus-effect"[9,10] and "petal-effect"[11] are typical phenomenon. The "lotus-effect" and "petal-effect" surfaces have same water-repellent character, while the "lotus-effect" surface has a self-cleaning phenomenon, and the "petal-effect" surface shows a high adhesive character. Therefore, those natural structures as mimetic models are always used to design and fabricate engineering materials surfaces. Fabrication of the bioinspired superhydrophobic surfaces has employed many methods, such as lithography,[12] sublimation,[13] template method,[14] chemical etching,[15,16] sol−gel methods,[17] electrochemical methods,[18] layer-by-layer methods,[19,20] bottom-up approach for fabrication of nanoarrays,[21] etc.

Recently, more and more researchers have focused their attention on fabricating hydrophobic films on metal materials. Aluminum and its alloys exhibit low density, excellent thermal and electrical conductivity, high specific strength, and good castability and thus become important structural materials for aerospace, automobile, building, and railway applications.[22] The fabrication of hydrophobic surface with micronano binary structure would be of great interest for improving the surface performance of aluminum alloys. Up to now, some methods have been reported for the fabrication of the superhydrophobic surface on aluminum alloy such as chemical etching,[23−27] sol−gel methods,[28,29] an anodization method,[30,31] electrochemical anodizing,[32] electrodeposition,[33] electrochemical machining,[34,35] self-assembly,[36] electrospinning,[37] a polymer replication method,[38] etc. However, the superhydrophobic surface with high adhesion on the aluminum alloy surface was rarely discussed. Inspired by rose petals, Bhushan et al.[39] fabricated the superhydrophobic surfaces with high or low adhesion by different methods to construct microstructure and nanostructure, respectively. The microstructure was prepared by a two-step molding process. The nanostructures on the microstructured sample was created by self-assembly of the alkane *n*-hexatriacontane ($CH_3(CH_2)_{34}CH_3$) deposited by a thermal evaporation method. Feng et al.[11] prepared biomimetic polymer films with well-defined nanoembossed structures by duplicating a petal's surface, which exhibited superhydrophobicity and high adhesion with a petal-effect. Sun et al.[40] fabricated a superhydrophobic surface with controlled adhesion based on the reaction between an alkyl thiol and hierarchical structured $Cu(OH)_2$ substrates. Yan et al.[41] created hydrophobic surfaces

Received: April 24, 2013
Accepted: August 7, 2013
Published: September 9, 2013

   dx.doi.org/10.1021/am4014715 | *ACS Appl. Mater. Interfaces* 2013, 5, 8907−8914

with high adhesive effect by assembling silica nanoparticles from the suspensions with different concentrations. Feng et al.[42] created an alumina surface with both superhydrophobicity and strong adhesion to water by the sol−gel method. Boscher et al.[43] fabricated fluorine-free surfaces with superhydrophobicity and high adhesion to water by the atmospheric pressure dielectric barrier discharge (APDBD) of hexamethyldisiloxane on cold rolled aluminum foil. Lee et al.[44] prepared a superhydrophobic aluminum surface with adhesiveness freely controlled within the range from highly adhesive to self-cleanable by two-step anodization. Guo et al.[45] fabricated a stable superhydrophobic surface with high adhesion on aluminum alloy by etching in NaOH aqueous solution and modifying with a PDMSVT + 1 wt % 184 curing agent inspired by the micronano binary hierarchical structures of lotus. However, the surfaces of the aluminum alloy become dark after etching by NaOH aqueous solution, and its application may be limited due to the brightness of surface being destroyed.

The superhydrophobic surfaces with high adhesion are promising due to their representative wetting behavior and relative research value in various realms, such as liquid transportation, microfluidic systems, barrier materials, lubricating materials, etc. Being an engineering material used widely, we believe that the superhydrophobic surface of aluminum alloy with high adhesion will be significant in industry due to the developed multifunctional surface. We present a facile, highly effective, and low-cost approach to fabricate the superhydrophobic aluminum alloy surface with high adhesive property.

In this article, a biomimetic superhydrophobic surface was fabricated via two-step methodology, which was processed by a laser and then immersed and etched in solution containing nitric acid and copper nitrate, and finally modified by DTS. Inspired by the hierarchical micronano-structure on the surface of plant leaves, the microscale crater-like pits and nanoscale reticula binary structure on an aluminum alloy were created, and the surface simultaneously had superhydrophobicity and adhesive property with petal-effect. Furthermore, the contact angle of superhydrophobic surfaces reached up to 158.8 ± 2°. The superhydrophobic surfaces showed excellent stability in an aqueous solution of pH 2−14 and after being exposed long-term, 3 months, in air.

2. EXPERIMENTAL DETAILS

2.1. Fabrication of Superhydrophobic Surfaces on Aluminum Alloy. Aluminum alloy (known as 3102Al in engineering materials), whose chemical composition included Si of 0.40 wt.%, Fe of 0.70 wt.%, Cu of 1.0 wt.%, Mn of 0.05−0.40 wt.%, Zn of 0.10 wt.%, Cr of 0.30 wt.%, Zr of 0.05 wt.%, other impurities of 0.15 wt.%, and the remaining element Al, with a size of 20 × 20 × 2 mm^3. The samples were first polished with No. 1000 SiC paper, followed by No. 1500 and No. 2000 to obtain a relatively smooth surface, and subsequently ultrasonically cleaned in absolute ethanol for 10 min and then dried. The microscale crater-like pits with a distance of 60 μm between adjacent pits central on the cleaned aluminum alloy surfaces were processed by a laser. The processed specimens were ultrasonically cleaned in absolute ethanol for 10 min. After being dried, the cleaned and processed aluminum alloy substrates were immersed and etched in the aqueous solutions of 4 mM/L $Cu(NO_3)_2$ and 5% HNO_3 at 80 °C for 1 min. After being cleaned ultrasonically in absolute ethanol for 10 min and dried, the samples were immersed in 60 mL of a toluene solution containing 600 μL of DTS ($CH_3(CH_2)_{11}Si(OCH_3)_3$) for 1 h. Finally, samples were cleaned ultrasonically in absolute ethanol for 10 min.

2.2. Surface Characterization. The morphologies of the aluminum alloy were observed by scanning electron microscope (JEOL JSM-7500F, Japan Electronic) at 15 kV and confocal laser scanning microscope (LEXT-OLS3000, Olympus, Japan). The surface chemical composition was examined by X-ray photoelectron spectroscopy (XPS, SPECS XR50). Static water contact angles of the fabricated surfaces were estimated with a contact angle meter (JC2000A Powereach, China) based on a sessile drop measuring method with a water drop volume of 3 μL. The chemical stability of the fabricated superhydrophobic surface in aqueous solutions at different pH values was examined by investigating the relationship between the pH values of aqueous solutions ranging from 1 to 14, and the static contact angles of the superhydrophobic surface were measured by dropping each aqueous solution's pH value. The long-term chemical stability of the superhydrophobic surface for storage in air for 3 months was also examined by investigating the relationship between changes in static water contact angles and time evolution after exposing the samples to air.

3. RESULTS AND DISCUSSION

3.1. Microstructure. Figure 1a shows the SEM morphology of the rose petal, where one can see periodic micropapillae close

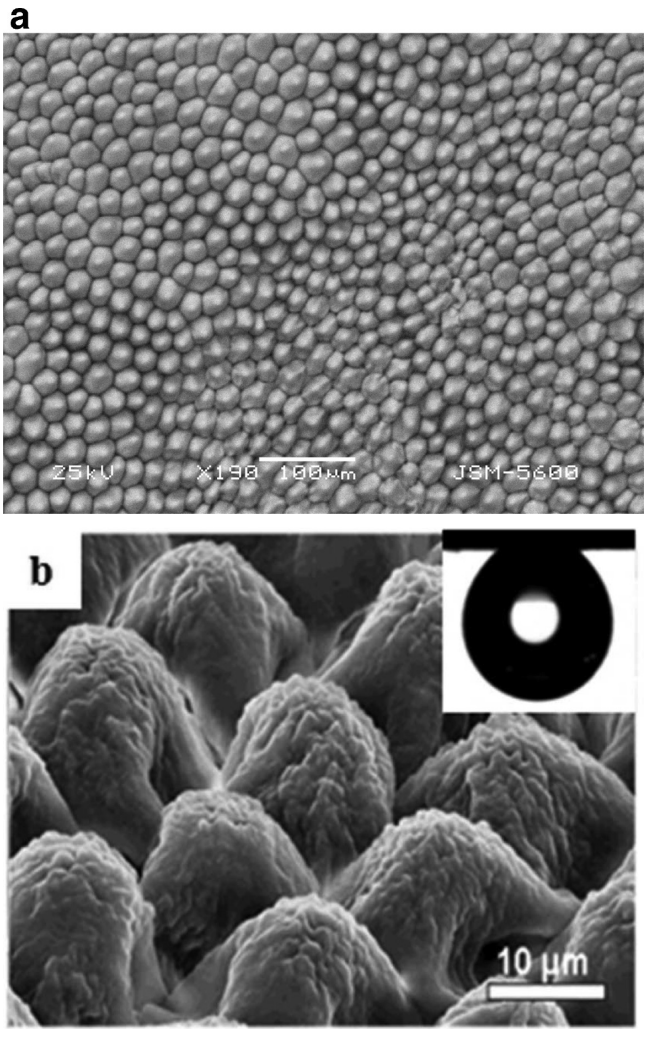

Figure 1. Morphology of the petal of red rose: (a) SEM image and (b) 3D image.[46]

arrays on the surface and nanoscale cuticular folds. Figure 1b shows the micropapillae with diameter ranges of 15 μm−18 μm and heights of 8 μm−10 μm, and these nanoscale cuticular folds on top of micropapillae with width ranges of 700−800 nm.[46] The hierarchical micronano binary structures endow the rose petals with sufficient roughness for superhydrophobicity with high

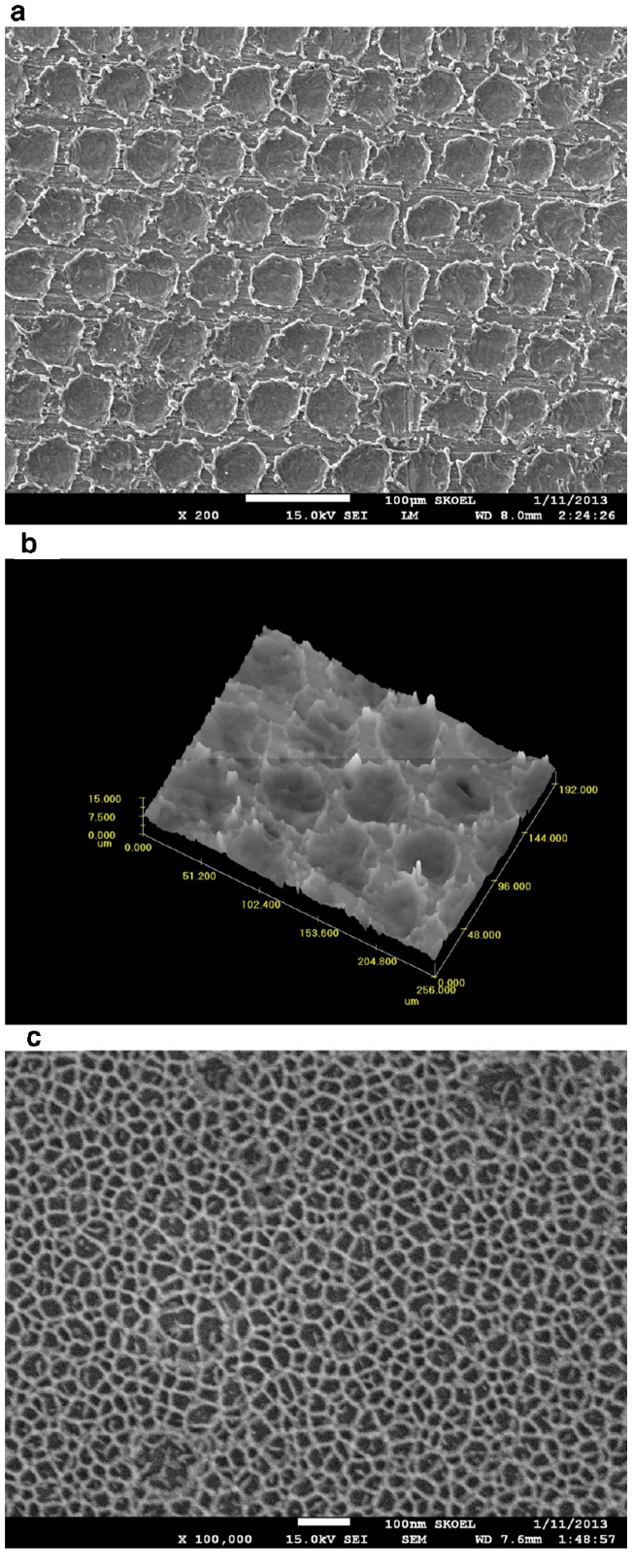

Figure 2. Morphology of the as-prepared surface on the aluminum alloy: (a) SEM image with microscale structure, (b) 3-D image by a confocal laser scanning microscope, and (c) SEM image with nanoscale structure after chemical etching.

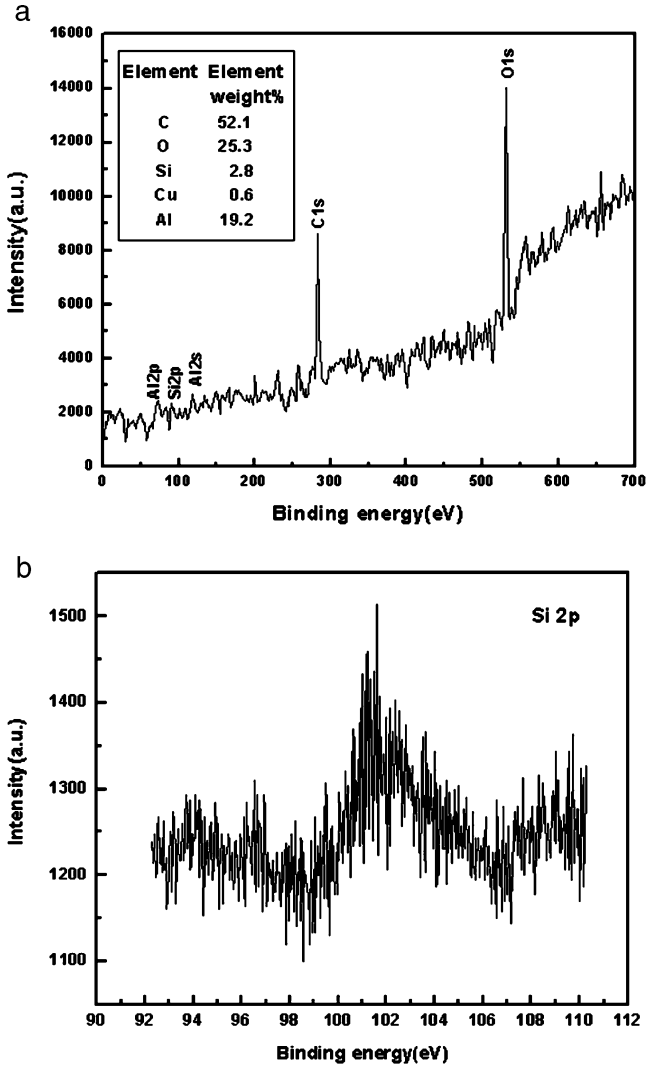

Figure 3. XPS spectrum of the as-prepared sample surface of a (a) full-spectrum and (b) Si 2p.

adhesive force to water.[11] A water droplet on the surface of these petals is a sphere, which cannot roll off even when turned upside down. Figure 2a shows the SEM image of an as-prepared surface myriad microscale crater-like pits with central distanced of 60 μm between adjacent pits by laser processing can be seen. Figure 2b shows the 3D morphology of the as-prepared surface with the depths of crater-like pits of 10 μm−15 μm. Figure 2c shows the SEM image of the as-prepared surface with nanoscale reticula structure by immersing and etching in the aqueous solutions of $Cu(NO_3)_2$ and HNO_3. No obvious changes on the morphology of the as-prepared surface are found before and after being modified in a toluene solution of DTS. The formation of nanoscale reticula structure may be due to the existence of a large number of dislocation defects in the aluminum alloy substrate and the chemical inertia of microelements. Figures 1b and 2b show the morphological characteristics of the rose petal and the as-prepared surface. There are different microstructures between the rose petal and as-prepared surface. The microstructure of the rose petal is microscale papillae, while the microstructure of the as-prepared surface is microscale crater-like. However, it can be clearly seen that the microstructure of the as-prepared surface is inverse the petal's structures with a close array of approximately hemispherical concaves. Therefore, the microstructure of the as-prepared surface is similar to that of the petal according to the geometric condition consisting of the micronano binary

dx.doi.org/10.1021/am4014715 | ACS Appl. Mater. Interfaces 2013, 5, 8907−8914

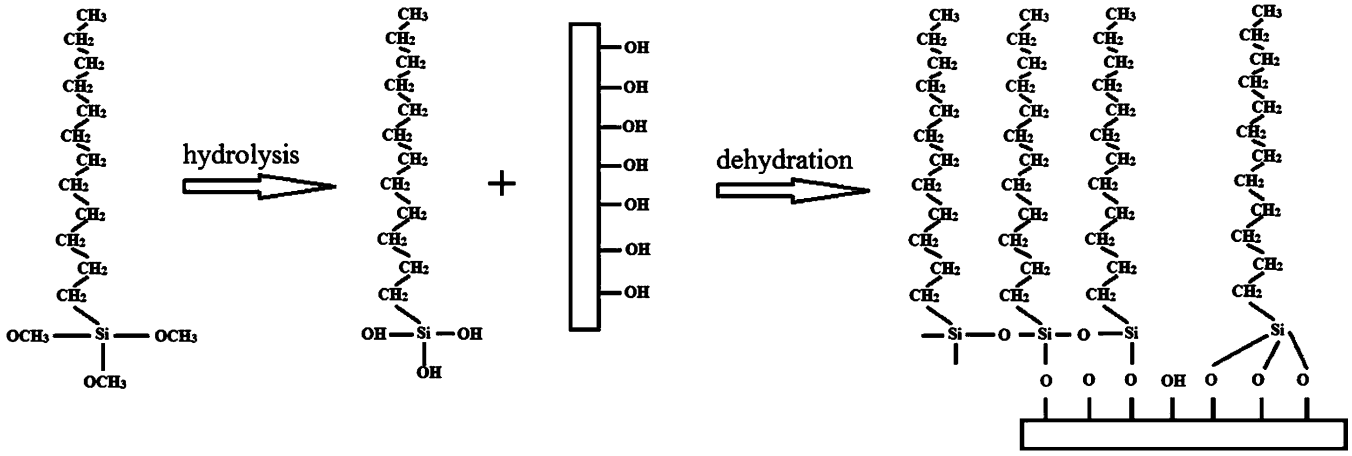

Figure 4. Formation scheme of the self-assembled DTS film on the aluminum alloy surfaces.

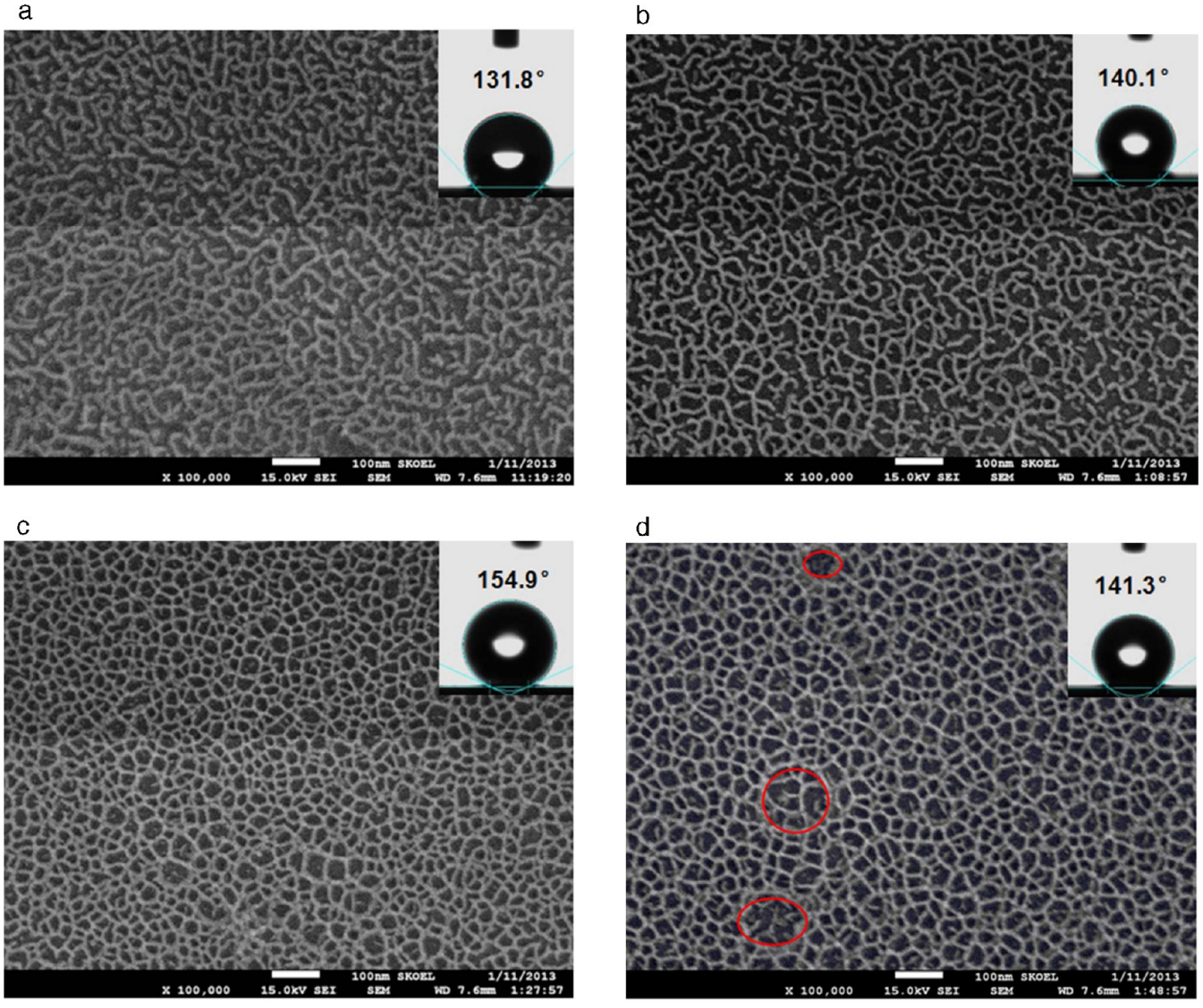

Figure 5. SEM images of the laser processing surfaces after etching for (a) 20, (b) 40, (c) 60, and (d) 90 s followed by modification with DTS.

structure. Therein, we can call the as-prepared surface as a biomimetic surface inspired by rose petals.

3.2. Chemical Conditions. XPS is used to test the chemical composition of the as-prepared surfaces modified by DTS after laser processing and etching. Figure 3 shows the XPS survey spectrum of the chemical composition on the modified surfaces. It reveals the presence of C, Si, O, and Al on the as-prepared surfaces. A strong peak of C1s at 283.5 eV and Si 2p at 102 eV can

dx.doi.org/10.1021/am4014715 | ACS Appl. Mater. Interfaces 2013, 5, 8907−8914

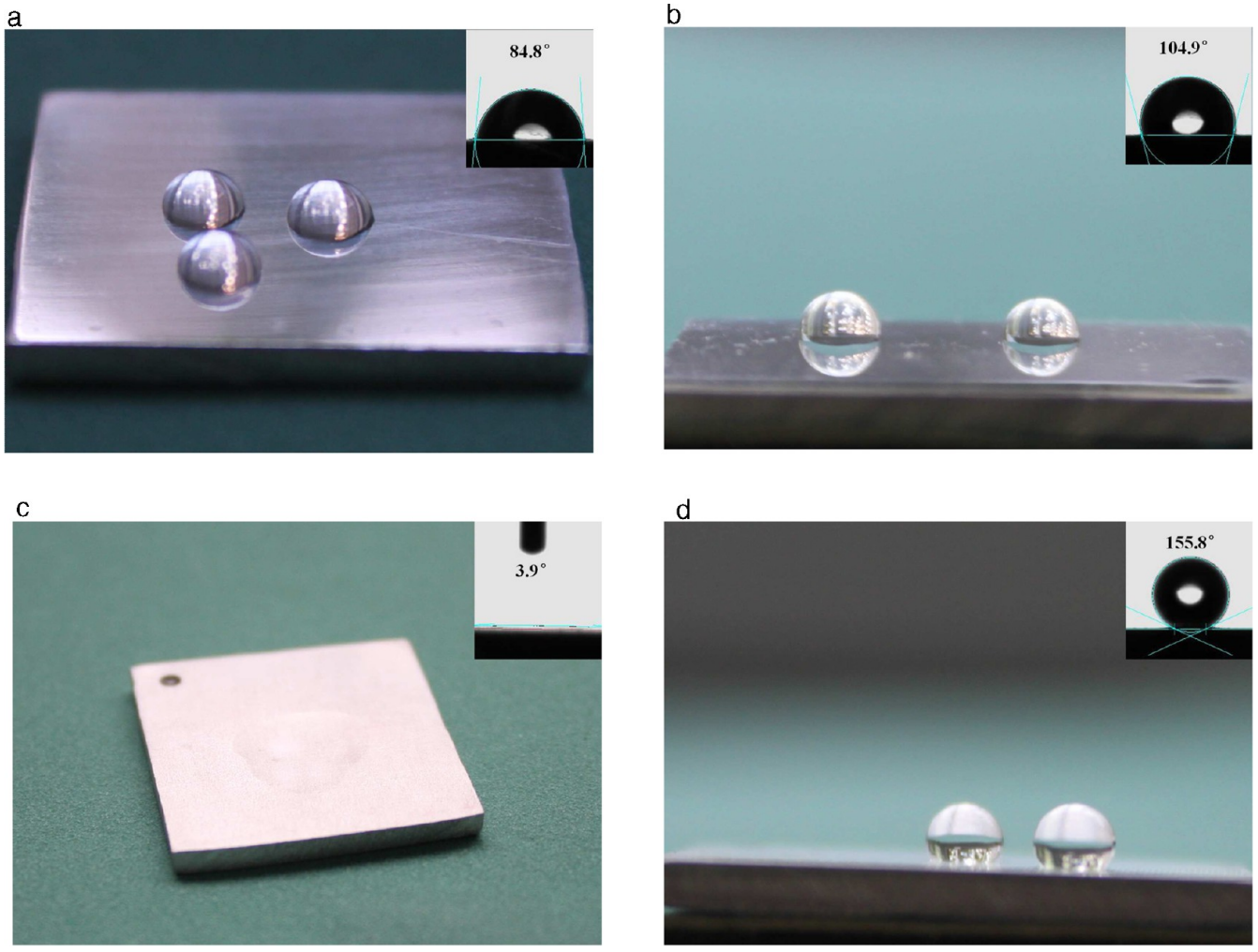

Figure 6. Photos of water contact angles on the aluminum alloy of (a) a flat surface before being modified with DTS, (b) the flat surface after being modified with DTS, (c) laser processing and etched surfaces before being modified with DTS, and (d) laser processing and etched surfaces after being modified with DTS.

been seen. The composition of Si and C increased remarkably compared to that of the substrate, which implied that the surface has been covered with silane film. Moreover, the Si 2p peak with a binding energy at 102 eV of the modified sample indicated DTS molecules grafted onto aluminum alloy substrates because this peak is well pronounced in the spectrum for the silanized sample.[47] It has been proved that the silane molecule can be strongly anchored to the aluminum substrate by the surface reaction of the hydrolysis silane species with the surface functional groups (Al−OH) of the aluminum substrate to form a self-assembled monolayer (SAM) with low surface energy.[48] Therefore, DTS molecules were speculated to form SAM on the roughened aluminum alloy surface through a similar way in our research, which would help to amplify the superhydrophobicity of the rough substrate.

Aluminum alloys are etched in the chemical etchants, which contain HNO_3 aqueous solution (eq 1). In the chemical etching solution, copper nitrate exists as copper ions (Cu^{2+}). Copper ions receive electrons from aluminum alloys and are reduced to copper particles (Cu) (eq 2). This process induces the formation of micro-orifices, which would accelerate the erosion of the surrounding aluminum.

$$Al + 4HNO_3 = Al(NO_3)_3 + NO\uparrow + 2H_2O \quad (1)$$

$$2Al + 3Cu^{2+} = 3Cu + 2Al^{3+} \quad (2)$$

Figure 4 shows the self-assembly of DTS on the aluminum alloy surfaces.[49] The surface energy decreases in the order $-CH_2- > -CH_3 > -CF_2 \rightarrow -CF_3$.[50] This is readily observed in the surface energies of polymer DTS, which contains the $-CH_3$ group with a surface energy of 24 mJ/m^2 and the $-CH_2-$ group with a surface energy of 31 mJ/m^2. These groups were used to reduce the free energy of the aluminum alloy surfaces. First, the silicon methoxide ($Si\text{-}OCH_3$) functional groups react with water to form silanols (Si-OH), which act as the reactive groups at the end of the molecule. The silanols subsequently react with the OH groups to form a self-assembled film. Meanwhile, the surface can also induce vertical polymerization to form a grafted polysiloxane.[51]

3.3. Etching Time. Highly uniform microscale structures were obtained by laser processing on aluminum alloy surfaces. Then, the samples were immersed and etched to obtain nanoscale structure. Figure 5 shows the samples were etched for 20 s, 40 s, 60 s, 90 s followed by modification with DTS and their water contact angles, which reach up to highest value when the samples were etched for 60 s. It is easy to see that reticular porous structures formed on the aluminum alloy surfaces after etching. However, compared to etching for 60 s, the reticular

dx.doi.org/10.1021/am4014715 | ACS Appl. Mater. Interfaces 2013, 5, 8907−8914

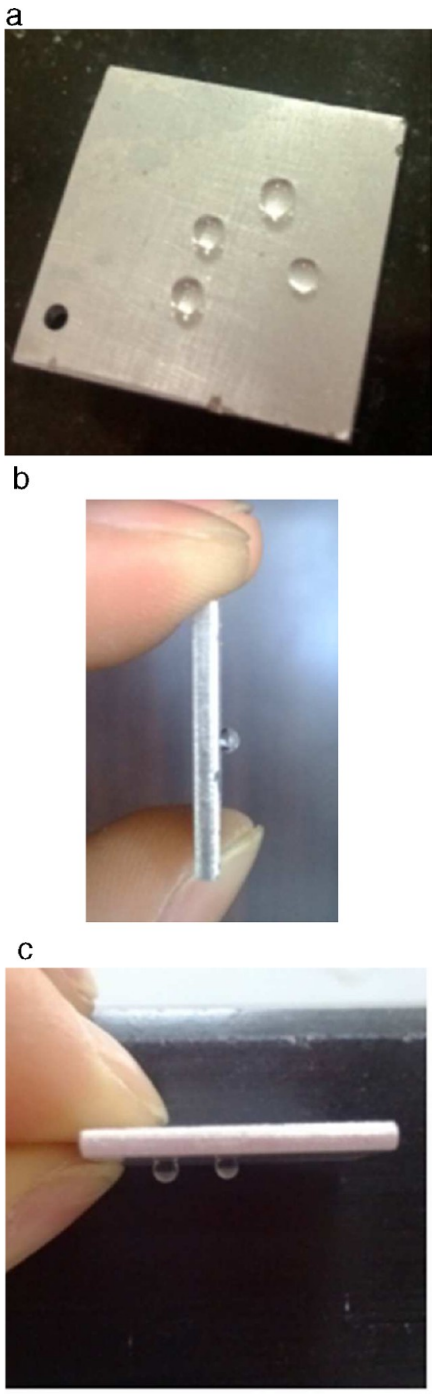

Figure 7. Images of water droplets of 3 μL on the as-prepared surface with different tilt angles: (a) 0°, (b) 90°, and (c) 180°.

structures of etching for 20 s and 40 s were intermittently distributed on the surface. When the etching time was extended to 90 s, however, a part of the reticular porous structures was destroyed (Figure 5d, the circled locations), leading to the reduction of the hydrophobicity. Therefore, 60 s was selected as the optimum time for etching.

3.4. Superhydrophobicity with High Adhesion. It is well known that an aluminum alloy is a type of hydrophilic engineering material with a native oxidized layer. Figure 6a shows photo of the water contact angle of a flat surface before being modified by DTS. The water contact angles of 3102Al were measured, and the average value is about 84.9 ± 2°. Figure 6b

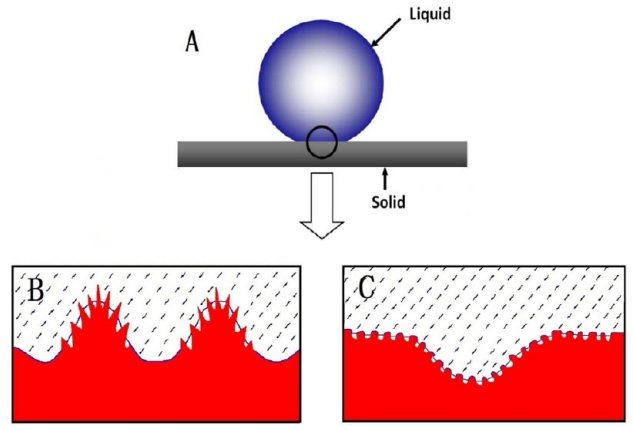

Figure 8. Schematic illustrations of a water droplet on the surface. (A) The model of a water droplet on the surface. (B) A drop of water in contact with the petal (Cassie impregnating wetting state). (C) A drop of water in contact with the binary structure.

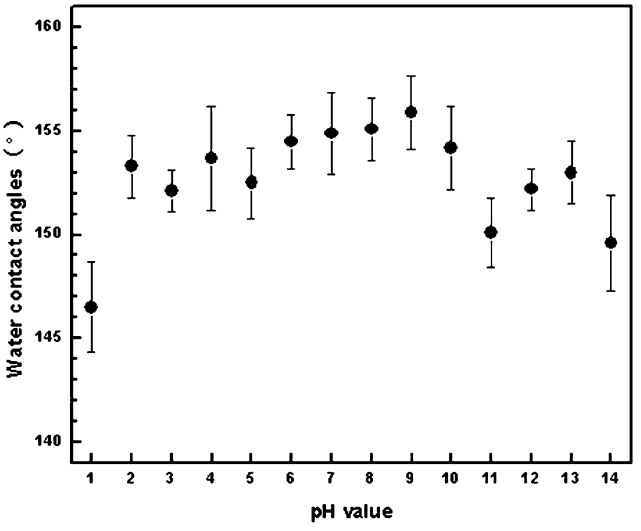

Figure 9. Relationship between pH values and static contact angles on the as-prepared surface.

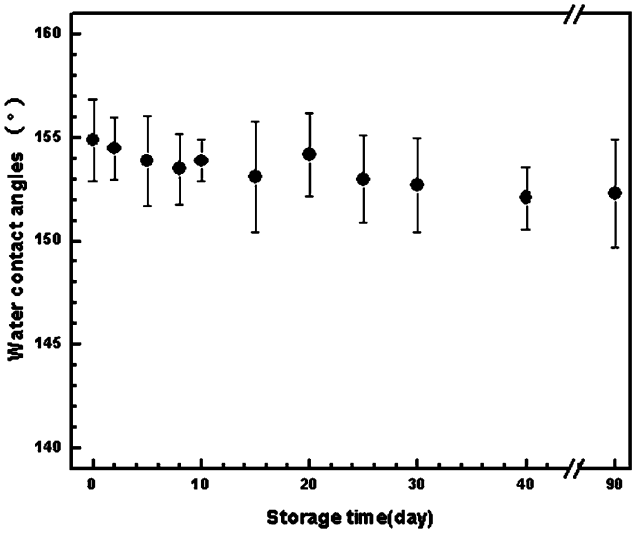

Figure 10. Water contact angles of the superhydrophobic surfaces after air exposure for different times.

dx.doi.org/10.1021/am4014715 | ACS Appl. Mater. Interfaces 2013, 5, 8907−8914

shows a photo of the water contact angle of a flat surface after being modified by DTS. After being modified with DTS, the contact angle of an aluminum alloy surface increases to 104.5 ± 2°. Figure 6c,d shows photos of the water contact angle of laser processing and etched surfaces before and after being modified by DTS. The contact angle of the as-prepared surface with micronano-binary hierarchical structures on the aluminum alloy is 3.9 ± 2° before being modified with DTS, while after being modified with DTS, the contact angle of the as-prepared surface reaches up to 158.8 ± 2°, and the average value of the water contact angle reaches as high as 156.5 ± 2°. The micronano binary hierarchical structures and chemical composition simultaneously play an important role in the hydrophobicity of a surface.

We also measured the contact angle hysteresis. Figure 7 shows that a water droplet on the surface of the as-prepared surface is spherical in shape and that it cannot roll off even when the surface is turned upside down, vertically, or is reversed. Similar to the petal-effect, this superhydrophobic surface shows a high adhesion force to a water droplet. It is believed that the surface tension force between the binary structure and the water droplet leads to the adhesive property. Given that the volume of the droplet was 3 μL, the adhesion force was determined to be at least 30 μL. Compared to the size of hierarchical micronano structures on the lotus-effect surface, the micronano structures on the petal-effect surface are much larger. The water droplet is expected to enter into the large grooves of the surface and steadily stay on the petal-effect surface even when the as-prepared surface is turned upside down. The volume of the droplet is the crucial parameter for this phenomenon. A small droplet whose weight is smaller than the surface tension force will stick to the surface. When the volume of the water droplet is about 12 μL, the weight of the water droplet and the surface tension reach a balance, and the droplet will fall.

To understand the superhydrophobicity with high adhesion behavior on the as-prepared surfaces, we carefully analyzed the mechanism affecting the adhesion. Usually, the petal-effect was explained by the Cassie impregnating wetting regime.[52,53] Figure 8b shows the schematic illustration of a water droplet on the rose petal, which is the typical Cassie impregnating wetting state. Figure 8c shows the schematic illustration of a water droplet on the as-prepared surface. On the surface with such microstructures, the water droplet can wet the big gaps between the microscale crater-like pits because of the large scale of the microstructures with a central distance of 60 μm; thus, a large liquid−solid contact area would emerge. Therefore, the surface has a high adhesion and can pin a water droplet due to the van der Waals force produced by the liquid−solid interface between the water droplet and the substrate. However, the water cannot wet the nanoscale reticular porous structure with a diameter of 40 nm−70 nm, and a large amount of air can be trapped in the porous structure, and the as-prepared surface shows superhydrophobicity.

3.5. Chemical Stability. The chemical stability of the superhydrophobic surface on aluminum alloys in aqueous solutions at different pH values was examined. Figure 9 shows the relationship between the pH and water contact angles of the as-prepared surface. The as-prepared surfaces show superhydrophobicity due to the water contact angles of more than 150° for aqueous solutions at pH 2−14. However, the contact angle for the most acidic droplets of a pH value of 1 is 146.5 ± 2°, and the as-prepared surface shows hydrophobicity. The results indicate that the as-prepared surface has good chemical stability in aqueous solutions of most acidic, alkali, and some aqueous salts. In addition, the long-term stability of the superhydrophobic surface for storage in air for 3 months was also examined by investigating changes in static water contact angles with time evolution. After storage in air for 90 days, the values of water contact angles reduce little as shown in Figure 10, indicating good stability in air.

4. CONCLUSIONS

In summary, biomimetic surfaces were fabricated via a two-step methodology, and the samples were processed by a laser and then immersed and etched in solution containing nitric acid and copper nitrate, and finally modified by toluene solution containing DTS. The superhydrophobic surfaces have a binary structure consisting of microscale crater-like pits and nanoscale reticula. The superhydrophobic surfaces are affected by micronano structure and chemical composition. The superhydrophobic surfaces with contact angles greater than 158.6 ± 2° are obtained. Especially, the surface with micronano binary structure had superhydrophobicity and adhesive properties simultaneously with a petal-effect. The superhydrophobic surfaces showed excellent stability in an aqueous solution of pH 2−14 and after being exposed a long-term of 3 months in air. The present work not only will be helpful in a systematic discussion about the wetting mechanism of superhydrophobicity with high adhesion but also will provide a new methodology to fabricate a multifunctional surface of aluminum alloy and even other metal materials.

AUTHOR INFORMATION

Corresponding Author

*Tel: +86 431 5095760. Fax: +86 431 5095575. E-mail: liuyan2000@jlu.edu.cn.

Notes

The authors declare no competing financial interest.

ACKNOWLEDGMENTS

We thank the National Natural Science Foundation of China (Nos. 51275555, 50905071, and 51201068) for financial support. Dr. Niu S.C. is gratefully acknowledged for his valuable discussions.

REFERENCES

(1) Han, Z. W.; Niu, S. C.; Shang, C. H.; Liu, Z. N.; Ren, L. Q. *Nanoscale* **2012**, *4*, 2879−2883.
(2) Wang, S. T.; Jiang, L. *Adv. Mater.* **2007**, *19*, 3423−3424.
(3) Liu, K. S.; Yao, X.; Jiang, L. *Chem. Soc. Rev.* **2010**, *39*, 3240−3255.
(4) Yan, Y. Y.; Gao, N.; Barthlott, W. *Adv. Colloid Interface Sci.* **2011**, *169*, 80−105.
(5) Nosonovsky, M.; Bhushan, B. *Adv. Funct. Mater.* **2008**, *18*, 843−855.
(6) Koch, K.; Bhushan, B.; Barthlott, W. *Soft Matter* **2008**, *4*, 1943−1963.
(7) Liu, K. S.; Jiang, L. *Nano Today* **2011**, *6*, 155−175.
(8) Xia, F.; Jiang, L. *Adv. Mater.* **2008**, *20*, 2842−2858.
(9) Gao, L. C.; McCarthy, T. J. *Langmuir* **2006**, *22*, 2966−2967.
(10) Miwa, M.; Nakajima, A.; Fujishima, A.; Hashimoto, K.; Watanabe, T. *Langmuir* **2000**, *16*, 5754−5760.
(11) Feng, L.; Zhang, Y. N.; Xi, J. M.; Zhu, Y.; Wang, N.; Xia, F.; Jiang, L. *Langmuir* **2008**, *24*, 4114−4119.
(12) Jung, Y. C.; Bhushan, B. *ACS Nano* **2009**, *3*, 4155−4163.
(13) Lai, Y. K.; Huang, Y. X.; Wang, H.; Huang, J. Y.; Chen, Z.; Lin, C. J. *Colloids Surf., B* **2010**, *76*, 117−122.
(14) Vayssieres, L. *Adv. Mater.* **2003**, *15*, 464−466.

(15) Liu, Y.; Lu, G. L.; Liu, J. D.; Han, Z. W.; Liu, Z. N. *Appl. Surf. Sci.* **2013**, *264*, 527−532.
(16) Han, M.; Go, S.; Ahn, Y. *Bull. Korean Chem. Soc.* **2012**, *33*, 1363−1366.
(17) Manca, M.; Cannavale, A.; Marco, L. D.; Arico, A. S.; Cingolani, R.; Gigli, G. *Langmuir* **2009**, *25*, 6357−6362.
(18) Wu, Z. Z.; Lee, D.; Rubner, M. F.; Cohen, R. E. *Small* **2007**, *3*, 1445−1451.
(19) Zhai, L.; Cebeci, F. C.; Cohen, R. E.; Rubner, M. F. *Nano Lett.* **2004**, *4*, 1349−1353.
(20) Niu, J.; Shi, F.; Liu, Z.; Wang, Z. Q.; Zhang, X. *Langmuir* **2007**, *23*, 6377−6384.
(21) Shi, F.; Niu, J.; Liu, Z.; Wang, Z. Q.; Smet, M.; Dehaen, W.; Qiu, Y.; Zhang, X. *Langmuir* **2007**, *23*, 1253−1257.
(22) Chen, L.; Wang, H. Y.; Luo, D.; Zhang, H. Y.; Liu, B.; Jiang, Q. C. *CrystEngComm* **2013**, *15*, 1787−1793.
(23) Saleema, N.; Sarkar, D. K.; Gallant, D.; Paynter, R. W.; Chen, X. G. *ACS Appl. Mater. Interfaces* **2011**, *3*, 4775−4781.
(24) Yin, B.; Fang, L.; Tang, A. Q.; Huang, Q. L.; Hu, J.; Mao, J. H.; Bai, G.; Bai, H. *Appl. Surf. Sci.* **2011**, *258*, 580−585.
(25) Sarkar, D. K.; Farzaneh, M.; Paynter, R. W. *Mater. Lett.* **2008**, *62*, 1226−1229.
(26) Liu, L. J.; Zhao, J. S.; Zhang, Y.; Zhao, F.; Zhang, Y. B. *J. Colloid Interface Sci.* **2011**, *358*, 277−283.
(27) Saleema, N.; Sarkar, D. K.; Paynter, R. W.; Chen, X. G. *ACS Appl. Mater. Interfaces* **2010**, *2*, 2500−2502.
(28) Xu, Q. F.; Wang, J. N. *New J. Chem.* **2009**, *33*, 734−738.
(29) Lu, S. X.; Chen, Y. L.; Xu, W. G.; Liu, W. *Appl. Surf. Sci.* **2010**, *256*, 6072−6075.
(30) Zhang, Y. F.; Yu, X. Q.; Wu, H.; Wu, J. *Appl. Surf. Sci.* **2012**, *258*, 8253−8257.
(31) Wang, H.; Dai, D.; Wu, X. D. *Appl. Surf. Sci.* **2008**, *254*, 5599−5601.
(32) Jeong, C. Y.; Choi, C. H. *ACS Appl. Mater. Interfaces* **2012**, *4*, 842−848.
(33) Huang, Y.; Sarkar, D. K.; Chen, X. G. *Nano-Micro Lett.* **2011**, *3*, 160−165.
(34) Song, J. L.; Xu, W. J.; Lu, Y. *J. Mater. Sci.* **2012**, *47*, 162−168.
(35) Xu, W. J.; Song, J. L.; Sun, J.; Dou, Q. L.; Fan, X. J. *J. Mater. Sci.* **2011**, *46*, 5925−5930.
(36) Park, B. G.; Lee, W.; Kim, J. S.; Lee, K. B. *Colloids Surf., A* **2010**, *370*, 15−19.
(37) Grignard, B.; Vaillant, A.; Coninck, J. D.; Piens, M.; Jonas, A. M.; Detrembleur, C.; Jerome, C. *Langmuir* **2011**, *27*, 335−342.
(38) Lee, Y. W.; Ju, K. Y.; Lee, J. K. *Langmuir* **2010**, *26*, 14103−14110.
(39) Bhushan, B.; Her, E. K. *Langmuir* **2010**, *26*, 8207−8217.
(40) Cheng, Z. J.; Du, M.; Lai, H.; Zhang, N. Q.; Sun, K. N. *Nanoscale* **2013**, *5*, 2776−2783.
(41) Gao, N.; Yan, Y. Y.; Chen, X. Y.; Mee, D. J. *Langmuir* **2012**, *28*, 12256−12265.
(42) Feng, L. B.; Liu, Y. H.; Zhang, H. X.; Wang, Y. P.; Qiang, X. H. *Colloids Surf., A* **2012**, *410*, 66−71.
(43) Nicolas, D. B.; David, D.; Stéphane, V.; Patrick, C. *ACS Appl. Mater. Interfaces* **2013**, *5*, 1053−1060.
(44) Lee, W. B.; Park, B. G.; Kim, D. H.; Ahn, D. J.; Park, Y.; Lee, S. H.; Lee, K. B. *Langmuir* **2010**, *26*, 1412−1415.
(45) Guo, Z. G.; Liu, W. M. *Appl. Phys. Lett.* **2007**, *90*, 223111.
(46) Park, Y. M.; Gang, M.; Seo, Y. H.; Kim, B. H. *Thin Solid Films* **2011**, *520*, 362−367.
(47) Cui, N. Y.; Liu, C. Z.; Brown, N. M. D.; Meenan, B. J. *Appl. Surf. Sci.* **2007**, *253*, 6932−6938.
(48) Fu, X. Y.; He, X. H. *Appl. Surf. Sci.* **2008**, *255*, 1776−1781.
(49) Liu, Y.; Yin, X. M.; Zhang, J. J.; Wang, Y. M.; Han, Z. W.; Ren, L. Q. *Appl. Surf. Sci.* **2013**, *280*, 845−849.
(50) Robert, F.; Brady, J. R. *Nature* **1994**, *368*, 16−17.
(51) Xu, W. J.; Song, J. L.; Sun, J.; Lu, Y.; Yu, Z. Y. *ACS Appl. Mater. Interfaces* **2011**, *3*, 4404−4414.
(52) Zhang, Y. L.; Chen, Q. D.; Jin, Z.; Kim, E.; Sun, H. B. *Nanoscale* **2012**, *4*, 4858−4869.
(53) Feng, L.; Zhang, Y. A.; Cao, Y. Z.; Ye, X. X.; Jiang, L. *Soft Matter* **2011**, *7*, 2977−2980.